Geophysical Research Letters®

Key Points:

- We assess the impact of subglacial-discharge plumes on water properties proximal to 14 tidewater glaciers in northwest Greenland
- In late summer, waters emanating from glacial plumes often make up >50% of the fjord water composition at intermediate depths
- These plume waters are comprised largely of upwelled Atlantic Water, warming the near-glacier water profile and likely increasing submarine melting

Author Contributions:

Conceptualization: T. R. Cowton
Data curation: T. R. Cowton
Formal analysis: T. R. Cowton, D. A. Slater, M. E. Inall
Funding acquisition: T. R. Cowton, D. A. Slater, M. E. Inall
Investigation: T. R. Cowton
Methodology: T. R. Cowton, D. A. Slater, M. E. Inall
Project Administration: T. R. Cowton
Resources: T. R. Cowton
Software: T. R. Cowton, D. A. Slater
Validation: T. R. Cowton
Visualization: T. R. Cowton

Subglacial-Discharge Plumes Drive Widespread Subsurface Warming in Northwest Greenland's Fjords

T. R. Cowton[1] ![ORCID], **D. A. Slater[2]** ![ORCID], **and M. E. Inall[3]** ![ORCID]

[1]School of Geography and Sustainable Development, University of St Andrews, St Andrews, UK, [2]School of Geosciences, University of Edinburgh, Edinburgh, UK, [3]Scottish Association for Marine Science, Scottish Marine Institute, Argyll, UK

Abstract Greenland's glacial fjords modulate the exchange between the ice sheet and ocean. Subglacial-discharge-driven plumes adjacent to glaciers may exert an important influence on fjord water properties, submarine glacier melting and the export of glacially-modified waters to the shelf. Here we use a numerical plume model in conjunction with observations from proximal to 14 glaciers in northwest Greenland to assess the impact of these plumes on near-glacier water properties. We find that in late summer, waters emanating from glacial plumes often make up >50% of the fjord water composition at intermediate depths. These plume waters are comprised largely of upwelled Atlantic Water, warming the near-glacier water profile and likely increasing submarine melting. Our findings demonstrate the key role played by plumes in driving water modification in Greenland's fjords, and the potential for simple models to capture these impacts across a range of settings.

Plain Language Summary Fjords form an important point of contact between the Greenland Ice Sheet and surrounding ocean. Warm ocean waters in these fjords melt the submerged sections of marine-terminating glaciers, whilst freshwater draining from the ice sheet modifies coastal water properties, impacting ocean circulation. In this study, we use observations of fjord temperature and salinity in combination with numerical modeling to evaluate the mechanisms through which glaciers modify fjord circulation and water properties. Across 14 glaciers in northwest Greenland, we find that the input of glacial meltwater drives the upwelling of warm, deep Atlantic-origin waters, which mix with the cooler Arctic-origin waters typically found above ~250 m depth. These glacially modified waters thus cause a substantial warming of fjord waters relative to those off the coast, a feedback that will amplify the oceanic melting of these glaciers.

1. Introduction

The interaction between the Greenland Ice Sheet and the ocean is a major coupling in the climate system, with the potential to influence ice loss and ocean circulation (Catania et al., 2020; Golledge et al., 2019). A key component in this exchange are the fjords surrounding the ice sheet, in which water properties can differ substantially from the adjacent continental shelf (Straneo et al., 2012). This modification is important, because it influences the properties of both the ocean waters reaching tidewater (marine-terminating) glaciers and the glacially modified waters exported to the shelf (Catania et al., 2020; Sutherland et al., 2018). Better understanding of this modification is thus critical for linking ocean temperatures with glacier submarine melt rates and glacial meltwater fluxes with ocean circulation. It has however proven challenging to constrain the impact of the various processes that influence fjord water properties, from the exchange mechanisms governing the renewal of fjord waters (e.g., Jackson et al., 2014; Zhao et al., 2021) to the ice and meltwater interactions modifying properties within the fjords (e.g., Davison et al., 2022; Mortensen et al., 2020).

The vast majority of meltwater generated at the ice sheet surface drains subglacially (Mankoff et al., 2020). At tidewater glaciers, this meltwater thus enters fjords at depth, rising buoyantly to form turbulent plumes which entrain ambient fjord waters until finding neutral buoyancy or reaching the surface (Jenkins, 2011). This upwelling drives an overturning circulation which helps maintain an up-fjord flow of warm subsurface waters toward glaciers (e.g., Cowton et al., 2016) and determines the depth and dilution at which subglacial discharge is exported from the fjord (e.g., Muilwijk et al., 2022). Modeling and indirect measurements indicate that currents generated by plumes directly increase submarine melt rates (e.g., Fried et al., 2019; Slater et al., 2016), which are further affected by changes to the temperature and salinity stratification of the fjord as a consequence of plume upwelling (e.g., Chauché et al., 2014).

Writing – original draft: T. R. Cowton
Writing – review & editing: T. R. Cowton, D. A. Slater, M. E. Inall

Observational studies have frequently identified temperature and salinity anomalies in Greenland's fjords, attributed to the effects of glacial modification (e.g., Inall et al., 2014; Mortensen et al., 2020; Straneo et al., 2011). It is however difficult to constrain the specific impacts of subglacial-discharge plumes and submarine ice melting based on hydrographic observations alone, reflecting challenges including scarce measurements of plume properties and the multiple source waters present in fjords (Beaird et al., 2015, 2018). Combining observations with numerical modeling of plume properties has proven advantageous in this respect, providing valuable insight into plume mechanics (Bendtsen et al., 2015; Jackson et al., 2017) and aiding with the interpretation of plume modification in individual fjords (Muilwijk et al., 2022; Stevens et al., 2016).

Nevertheless, if the effects of glacial modification on ice sheet—ocean interaction are to be more fully accounted for, an assessment of these impacts across a diverse range of fjords is required. Here, we combine numerical plume modeling with hydrographic observations from NASA's Ocean's Melting Greenland (OMG) mission to characterize and quantify the impacts of subglacial-discharge plumes on near-glacier hydrography at 14 tidewater glaciers in northwest Greenland over a period of five years. This provides a novel and wide-ranging assessment of the impact of glacial modification across one of Greenland's most heavily-glaciated coastlines.

2. Methods

To evaluate the form and causes of near-glacier water modification, we consider three sets of water properties: (a) from close to the terminus of each study glacier; (b) from the continental shelf adjacent to each study glacier; and (c) of the plume modified water (PMW) generated by subglacial-discharge plumes at each study glacier.

2.1. Near-Glacier and Shelf Water Properties

We select 14 glaciers in northwest Greenland, based on the availability of contemporaneous OMG Conductivity-Temperature-Depth (CTD) data from near to the glacier and on the adjacent shelf (Figure 1a) (Fenty et al., 2016; OMG, 2020). Data is available from five glaciers in 2016, one in 2017, five in 2018, eleven in 2019 and nine in 2020, and is available from August to October only (Figure 1b).

To obtain near-glacier water properties (water type 1, above), we select the closest CTD to each of the named glaciers (Figure 1, Table S1 in Supporting Information S1). We do not consider across-fjord variability, which we assume to be small compared to fjord-to-shelf differences (e.g., Muilwijk et al., 2022). The distance from the named glacier to the near-glacier CTD ranges from <1 to 16 km (median 5 km) (Table S1 in Supporting Information S1). To obtain the corresponding shelf water properties (water type 2, above), we select a second CTD cast for each glacier, lying close to the fjord mouth or on the cross-shelf trough (Figure 1a). In most cases the shelf and the near-glacier cast were recorded within 1–2 days (maximum difference of 6 days; Table S1 in Supporting Information S1), and we attribute differences between these to be due to spatial rather than temporal variability in water properties. We convert all values to Absolute Salinity (S, g kg^{-1}) and Conservative Temperature (Θ, °C), henceforth referred to as salinity and temperature, using the TEOS10 Gibbs-SeaWater Oceanographic Toolbox (McDougall & Barker, 2011).

For context, we additionally extract monthly temperature data for this region from Hadley Centre EN.4.2.2 temperature objective analyses (including .g10 bias corrections) (Good et al., 2013, 2023; Gouretski & Cheng, 2020; Gouretski & Reseghetti, 2010) (Figure 1b and Figure S1 in Supporting Information S1). We exclude months where the stated observation weight is <0.6 at the sample location (where ~1 shows observations have strongly influenced the analysis, and 0 indicates no observations were available).

2.2. Plume Modified Water

As direct observations of PMW properties are scarce, we model these using a buoyant plume model (Slater et al., 2016), forced with subglacial discharge, grounding line depth and ambient water properties. Similar models have been used extensively for tidewater glaciers (e.g., Carroll et al., 2016; Jenkins, 2011), and perform well when tested against observations (Jackson et al., 2017; Mankoff et al., 2016).

We use data from BedMachine v5 (Morlighem et al., 2017, 2023) to approximate the depths of glacier grounding lines and the shallowest sills between each of the paired shelf and near-glacier CTD casts, as well as to delimit
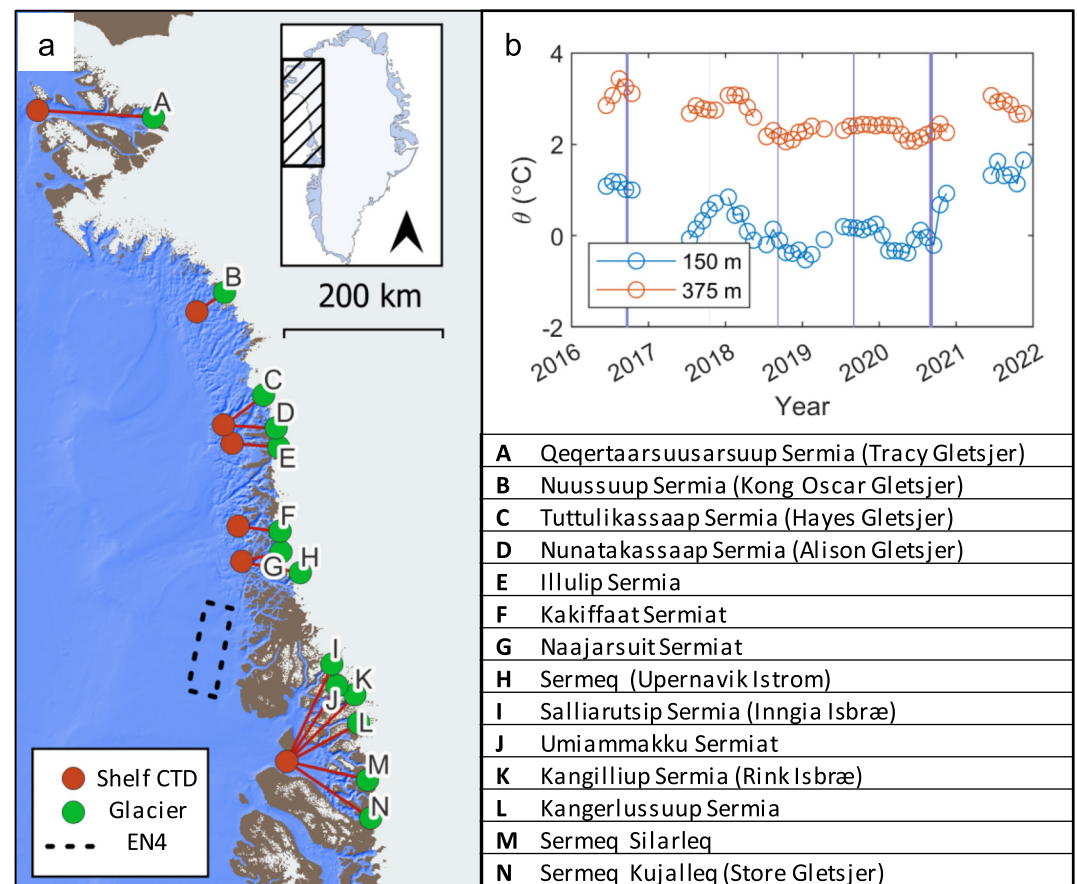
Figure 1. (a) Location and names (Bjørk et al., 2015) of study glaciers (green) and shelf CTDs (red) (Table S1 in Supporting Information S1). Near-glacier CTD locations overlap with glacier locations and are not shown. (b) EN.4.2.2 shelf subsurface water temperature (Good et al., 2013) ($1 \times 1°$ cell marked by dashed rectangle in (a)). Vertical bars in (b) show times during which CTD observations were obtained.

glacier catchments based on the hydraulic potential gradient from ice surface and bed topography (Shreve, 1972). We estimate timeseries of subglacial discharge (Figure S2 in Supporting Information S1) based on daily ice sheet surface runoff outputs from the regional climate model RACMO2.3, statistically downscaled to 1 km resolution (Noël et al., 2016), summed over the catchment of each glacier and assumed to enter the ocean with minimal delay.

Following Jackson et al. (2017), we use a "truncated line plume" geometry of 200 m width, though a point source of buoyancy (Slater et al., 2016) gives similar results (not shown). We assume that all runoff enters fjords subglacially at the maximum grounding line depth, and allow the plume to overshoot the point of neutral buoyancy, terminating when the momentum decreases to zero or the plume reaches the fjord surface. We then calculate the depth of neutral buoyancy based on the plume's final density relative to the equivalent near-glacier profile. We run the plume model only for the named glaciers, though we recognize that near-glacier CTD profiles may also be influenced by other glaciers terminating nearby.

To estimate PMW properties, we run the plume model for each glacier based on the subglacial discharge at daily intervals through each melt season, using both the near-glacier and shelf temperature and salinity profiles as ambient conditions. Although the former is closest to the location of the modeled plumes, the latter allows us generate PMW properties independent of PMW already present in the near-glacier observations. In practice, these approaches produce similar results and we focus on those generated using shelf profiles, with equivalent results based on near-glacier profiles shown in Supporting Information S1. To account for obstruction of deep water ingress into fjords, we replace below-sill shelf temperature and salinity profiles with sill-level values (e.g., Morlighem et al., 2019), and extrapolate these down to the grounding line depth when necessary.

For a given subglacial discharge, the plume model allows us to derive the depth at which the plume is predicted to reach neutral buoyancy, and the volume flux, temperature and salinity of the PMW input to the fjord from the plume at this depth. As subglacial discharge varies over the melt season, this traces out a vertical profile of PMW input volume and properties, which can be compared directly to the equivalent profiles of shelf and near-glacier water properties. Because we are restricted to a single survey per year, we are unable to incorporate the evolution of ambient conditions on sub-annual timescales. The accuracy of modeled PMW properties, and the impact of this PMW input on the recorded near-glacier water properties, thus both likely increase toward the point of acquisition of observations in late summer/fall.

2.3. Mixing Model

As subglacial-discharge plumes find neutral buoyancy and spread out into the fjord, PMW will be intruded into and mixed with ambient waters of similar density to itself. Where these plumes are the dominant mechanism of water modification, near-glacier waters in a given density class should therefore primarily comprise waters of shelf origin mixed with intruded PMW of similar density. We can therefore use a simple linear mixing model, based on temperature and salinity as conservative tracers, to derive the ratio of shelf waters and PMW required to generate the observed near-glacier water properties.

To do this we solve (in a least-squares sense) for the fraction F of PMW ($F_p(\rho)$) and shelf water ($F_s(\rho)$) giving the best fit to $\Theta_g(\rho)$ and $S_g(\rho)$, where subscripts g, s, and p denote near-glacier, shelf, and PMW respectively, and (ρ) denotes water masses of equal density:

$$\theta_g(\rho) = F_p\theta_p(\rho) + F_s\theta_s(\rho) \tag{1}$$

$$S_g(\rho) = F_pS_p(\rho) + F_sS_s(\rho) \tag{2}$$

$$F_p(\rho) + F_s(\rho) = 1 \tag{3}$$

We normalize Θ and S values with respect to the range encountered across the three water types in each density class (Supporting Information S1), and discard results where the sum of the squared residuals is $>10^{-2}$ (50% of cases), indicating that the near-glacier water properties cannot be satisfactorily reproduced within the assumptions of the mixing model. The majority of the retained results are located between ~100 and 300 m depth (Figure S3 in Supporting Information S1).

3. Results

Shelf water properties align with the main shelf water masses typically observed in this region (e.g., Muilwijk et al., 2022) (Figure 2a). At depth there is a layer of warm (0.0–3.0°C), salty (34.2–34.8 g kg^{-1}) Atlantic Water (AW), overlain by an intermediate layer of cooler (−1.3 to 1.3°C), fresher (33.3–34.2 g kg^{-1}) Polar Water (PW), both of which cool with increasing latitude. Above these lies a typically warmer and fresher surface layer. Based on these water masses and for the purposes of our analysis, we divide profiles into upper ($\sigma_\Theta < 26.6$ kg m^{-3}), intermediate ($26.6 \leq \sigma_\Theta < 27.3$ kg m^{-3}), and deep ($\sigma_\Theta \geq 27.3$ kg m^{-3}) layers (Figure 2a).

Near-glacier water properties are distinct from those on the shelf (Figure 2). The upper layer is typically cooler and fresher in the near-glacier profiles relative to those from the shelf, with mean differences (near-glacier minus shelf) of $\Delta\Theta = -2.84°C$ and $\Delta S = -0.38$ g kg^{-1} across all years (Figures 2c and 2d). The intermediate layer is conversely typically warmer ($\Delta\Theta = 0.34°C$) and saltier ($\Delta S = 0.03$ g kg^{-1}) in the near-glacier profiles during years 2016–2019, switching to slightly cooler ($\Delta\Theta = -0.14°C$) and fresher ($\Delta S = -0.01$ g kg^{-1}) in 2020. In the deep layer, near-glacier waters are slightly cooler ($\Delta\Theta = -0.18°C$) and fresher ($\Delta S = -0.11$ g kg^{-1}), particularly where sills block the flow of warm, salty water into fjords at depth.

There is a close agreement between PMW profiles modeled using the shelf and near-glacier profiles as ambient conditions in the plume model (Figure 3), due to the similarities between shelf and near-glacier properties across the deep layer in which the plume is predominantly entraining (Figures 2 and 3). Most PMW is predicted by the plume model to find neutral buoyancy in the intermediate and upper layers (Figure 4), and within these layers the similarity between the modeled PMW temperature profiles and the near-glacier profiles is in many cases striking (Figure 3 and Figure S9–18 in Supporting Information S1).
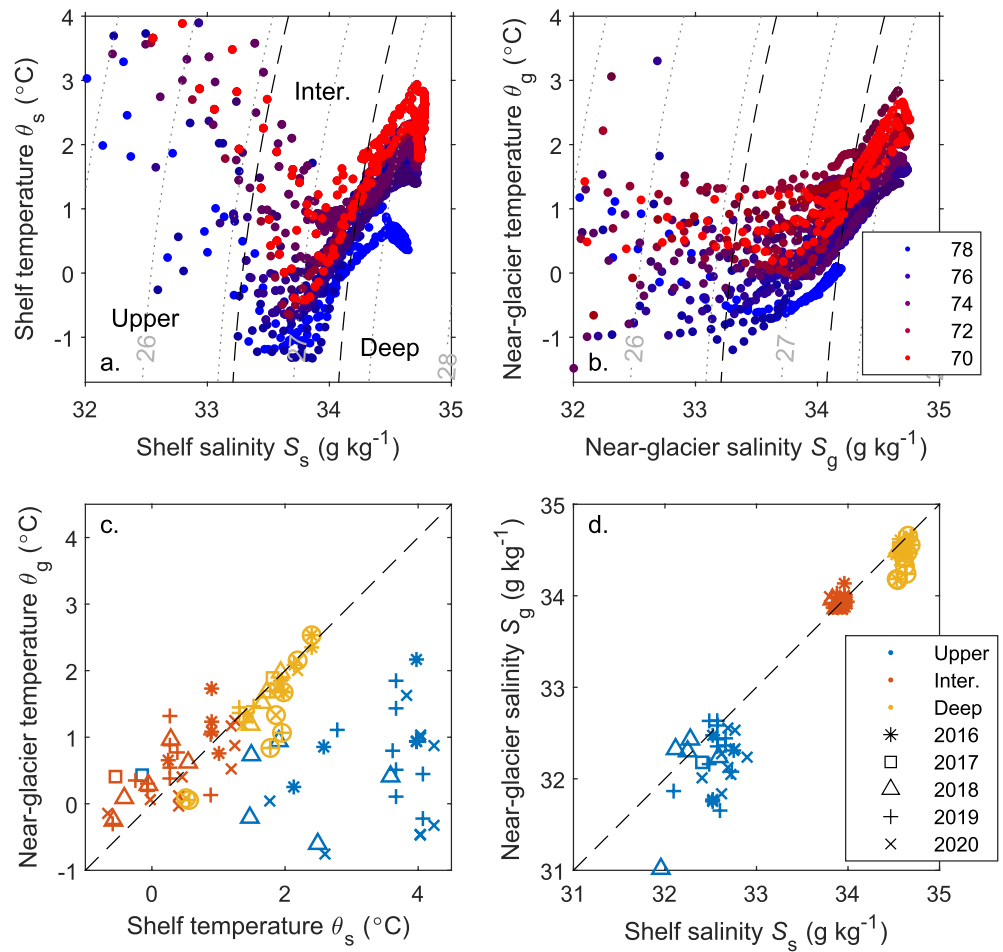
Figure 2. (a, b) Temperature—salinity plots for all (a) shelf and (b) near-glacier profiles. Color scale shows the latitude of observations (°N), with σ_Θ isopycnals (0.5 kg m^{-3} intervals) in gray. Dashed lines show boundaries between layers. Axis limits do not show the full extent of the upper layer. (c, d) Comparison of mean layer (c) temperature and (d) salinity between the shelf and near-glacier profiles for all locations and years. Encircled deep layer markers show sill depths ≤300 m.

PMW fractions, calculated for all near-glacier profiles using the mixing model, are shown in Figure 4 and Figure S4 and S5 in Supporting Information S1. Values of PMW >0.5 (where 1 is pure PMW) are obtained near to many glaciers, with maximum concentrations in the intermediate layer (Figure 4). The fraction of PMW decreases to close to zero below ∼500 m and at the surface, depths at which the modeled input of PMW is also limited (Figure 4). Sensitivity experiments show that uncertainty in grounding line depth, plume width, the plume entrainment coefficient and subglacial discharge predominantly affect the vertical distribution of PMW, whilst uncertainty in water properties predominantly affects the calculated PMW fractions (shading in Figure 4; Supporting Information S1).

4. Interpretation

PMW properties represent an integration of water properties between the grounding line and terminal depth of the plume. Plumes reaching the upper layer contain a mix of PW and AW, and can partly explain the cooling of this layer relative to the seasonally-warmed surface waters on the shelf (e.g., Figures 3b and 4l). The greatest impact is however observed in the intermediate layer, where plumes contain a high concentration of AW and are thus warm relative to the PW that otherwise dominates this layer (Figures 2 and 3). This plume-driven warming is seen in all years except 2020 and is most marked for glaciers at the southern end of the transect, where near-glacier waters are as much as ∼2°C warmer than shelf waters at equivalent depth (Figure 3). In 2020, near-glacier temperatures are contrastingly cooler than those on the shelf through much of the depth profile (Figure 2c and Figure S17 in
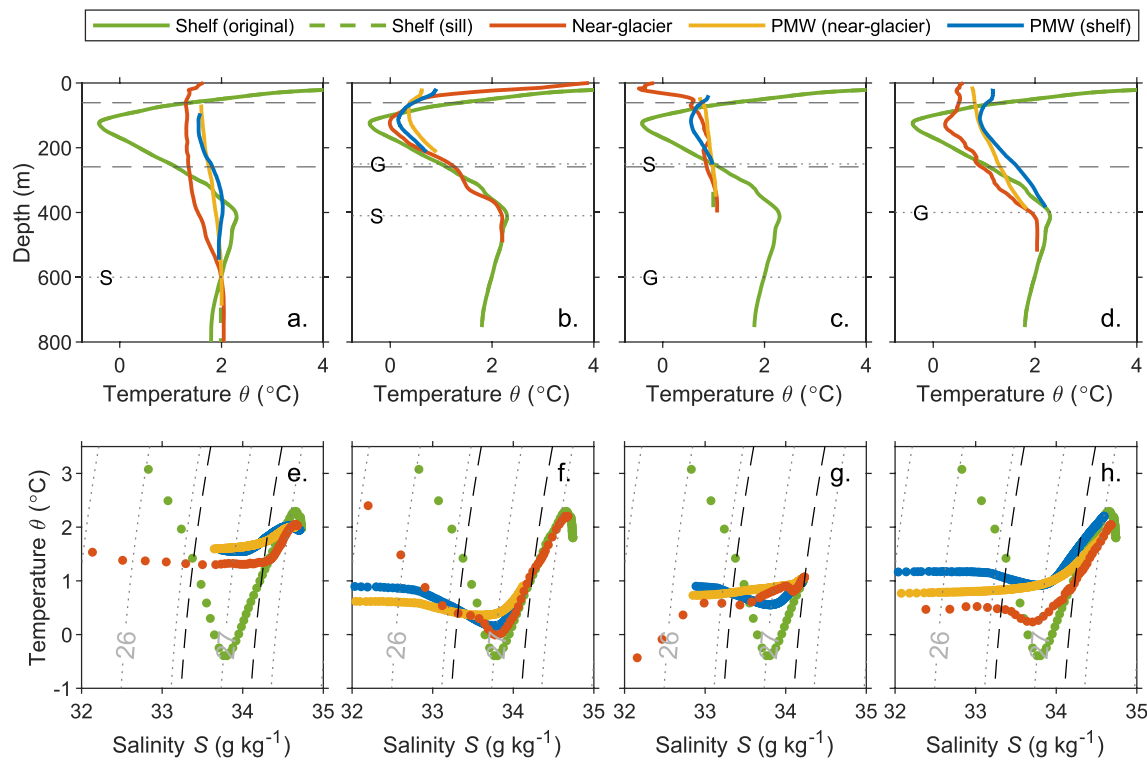
Figure 3. (a–d) Temperature profiles and (e–h) temperature-salinity plots for four example glaciers around Uummannaq Bay in 2019 (K-N respectively, Figure 1). Plots (a, c, e, and g) include extrapolation of the shelf profile below sill depth. Blue and yellow denotes PMW profiles modeled based on shelf and near-glacier water properties respectively. In (a–d), dotted lines show the depth of the shallowest sill (S) and the grounding line (G) (840 m in (a)). In (e–h), dots show data at 10 m depth intervals, with σ_Θ isopycnals (0.5 kg m^{-3} intervals) in gray. Black dashed lines show boundaries between layers (in a-d, based on shelf density profiles). Profiles for all glaciers and years are shown in Supporting Information S1.

Supporting Information S1). This may be explained by a sharp warming of shelf waters shown in the EN.4.2.2 data in fall 2020 (Figure 1b and Figure S1 in Supporting Information S1), which may not have been transmitted into fjords by the time of the survey. This results in comparatively little PMW being identified by the mixing model in 2020 (Figure S5 in Supporting Information S1), highlighting one of the challenges of relying on annual snapshots of shelf and near-glacier conditions.

Integrated over the summer, the greatest input of PMW is predicted by the plume model to occur at a shallower depth (∼50 m) than the peak concentrations of PMW identified by the mixing model (∼175 m) (Figure 4o). This may be in part due to the timing of observations in late summer/fall, when discharge decreases and plumes reach neutral buoyancy at greater depths (Figure S8 in Supporting Information S1). It is thus possible that the impact of PMW on the intermediate layer may be reduced during peak summer, when PMW input is typically concentrated around the upper–intermediate layer interface (Figure S8 in Supporting Information S1), though we note that observations from fjords adjacent to glaciers J-K (Figure 1) in July–August 2014 also show a marked warming of the intermediate layer relative to the shelf (Bartholomaus et al., 2016, their Figure 2). While PMW input may typically be greatest around the upper–intermediate layer interface, it is likely that this also drives a relatively rapid fjord-shelf exchange at this depth (e.g., Cowton et al., 2016), which may prevent high concentrations of PMW being maintained. Compared to within the intermediate layer, the temperature of PMW is also relatively similar to that of shelf waters around the upper-intermediate layer interface (Figure 3 and Figures S9–18 in Supporting Information S1), reducing its impact on fjord water properties at this depth. Additionally, the presence of PMW may be masked by processes (such as ice melt, terrestrial runoff input and atmospheric exchanges) occurring predominantly in the upper layer. This is reflected in the spike in the number of results failing the mixing model residual threshold above ∼100 m depth (Figure S3 in Supporting Information S1), indicating that the two component mixing model does not adequately reflect the processes contributing to water modification at these depths.

The concentration and distribution of PMW also varies between locations (Figure 4). To examine controls on this, we tested for Spearman's rank correlation between PMW depth (calculated as the mean depth of the PMW
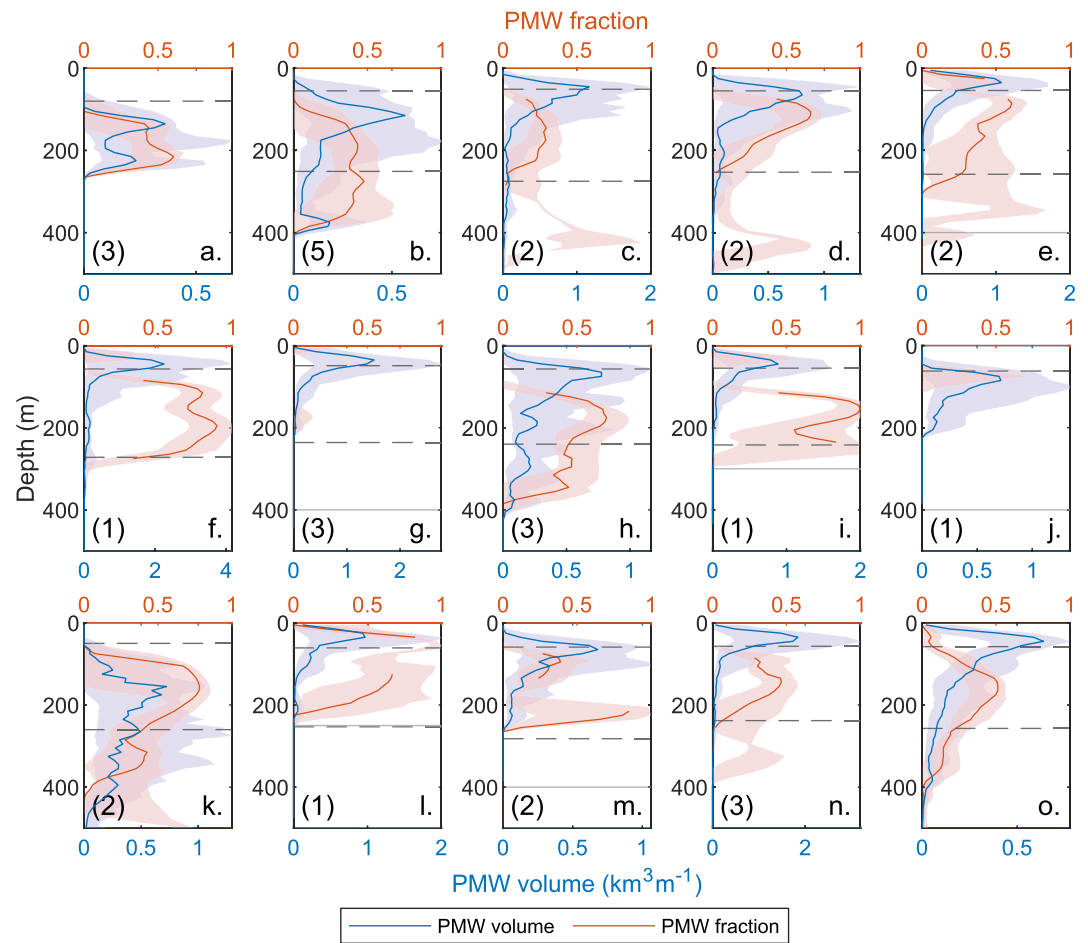
Figure 4. Modeled volume of PMW input annually per vertical meter of the water column, and calculated fraction of PMW present in near-glacier waters. Plots (a–n) relate to glaciers A-N in Figure 1, and show the mean of all data available across all years at that location. The mean of all years and locations is shown in (o). Lines show results for standard model parameter values, while shading shows the uncertainty range based on sensitivity experiments (Supporting Information S1). All curves are smoothed using a centered 30 m moving average. Dashed lines delimit layers based on the mean of the near-glacier density profiles at each location, and solid gray lines show grounding line depths (when <500 m). Numbers in (a–n) show the number of years of data at each location.

fraction distribution) and abundance (calculated as the depth-integrated PMW fraction) and key variables in the glacier/fjord system (Table S3 in Supporting Information S1). We find a positive correlation between PMW depth and grounding line depth ($r = 0.58$, $p < 0.05$), with shallower grounding lines helping plumes to reach shallower depths (e.g., Carroll et al., 2016). We do not however find a correlation between PMW abundance and distance of the observations from the glacier terminus, total annual subglacial discharge, or measures of fjord length, width or sill depth. While these factors may be expected to influence the input and dispersal of PMW (e.g., Carroll et al., 2017), it may be that this effect is masked by the relatively small sample population, uncertainties inherent in the models, and challenges in accurately quantifying PMW presence and complex fjord geometry as simple metrics (Slater et al., 2022).

5. Discussion

We find that intermediate layer water properties can frequently be explained as an approximately equal mixture of PMW and shelf PW, whilst alternative processes (such as submarine ice melt) become increasingly important toward the fjord surface. This agrees with studies from Upernavik Fjord (H in Figure 1; Muilwijk et al., 2022) and Sermilik Fjord, east Greenland (Beaird et al., 2018), both of which found high concentrations (>50%) of upwelled AW and low concentrations (<0.3%) of submarine melt water at intermediate depths. Our findings demonstrate

that this high concentration of relatively warm PMW at intermediate depths is characteristic of a wide range of locations along Greenland's northwest coast, highlighting a key driver of summer water modification proximal to Greenland's tidewater glaciers.

Of particular interest is the extent to which water temperatures adjacent to tidewater glaciers, key to determining submarine melt rates, differ from those on the shelf (Catania et al., 2020; Slater et al., 2020). We find that in most cases the temperature of the deep layer is similar between shelf and near-glacial profiles, except where sills serve to block in the ingress of water (Figures 2 and 3 and Figures S9–S18 in Supporting Information S1). Contrastingly, we find that at the time of the surveys in late summer/fall, plume-driven upwelling of AW has substantially warmed the intermediate layer adjacent to glaciers (at times by as much as 2°C relative to the shelf), whilst the surface layer is cooled relative to the shelf (Figures 2 and 3). These modifications will affect both the total submarine melting and the vertical distribution of melt (which may in turn affect calving rates (O'Leary & Christoffersen, 2013; Slater et al., 2021)) compared to melt rates calculated based on shelf temperatures alone, and should be considered when modeling the oceanic forcing of tidewater glaciers (e.g., Slater et al., 2020).

Meltwater from the Greenland Ice Sheet may have a profound impact on ocean circulation if it serves to freshen surface waters in deep water formation sites, weakening the AMOC (Golledge et al., 2019; Swingedouw et al., 2022). Our results illustrate however that subglacial discharge from major tidewater glaciers usually finds neutral buoyancy below the fjord surface (with PMW input rates peaking around 50 m depth), with the addition of freshwater counteracted by the upwelling of and mixing with deep, salty AW. As such, while the efficacy of plume entrainment amplifies the volume of PMW by two orders of magnitude relative to the subglacial discharge (Slater et al., 2022), it limits the freshening effect of this input. While there is a substantial freshening of the upper layer of the near-glacier profiles relative to the shelf (Figure 2d), this is not explained by the major subglacial discharge inputs modeled in this study, which produce sub-surface terminating plumes of similar salinity to ambient waters (Figures S9–S18 in Supporting Information S1). Instead it is likely to be driven by a combination of submarine melting of glacier termini and icebergs (e.g., Beaird et al., 2018), shallower surface-terminating subglacial-discharge plumes (at smaller glaciers or the periphery of larger glaciers) and surface runoff inputs.

6. Summary

We have analyzed hydrographic observations from proximal to 14 tidewater glaciers in northwest Greenland over the period 2016–2020. By comparing paired profiles from the shelf and near-glacier environment with modeled subglacial-discharge plume properties, we have characterized and quantified the impact of plume upwelling on near-glacier water properties. Whilst the greatest input of PMW occurs around 50 m depth, we find the strongest influence of plumes on fjord water properties within the intermediate layer (∼50–250 m), where PW is mixed with and displaced by PMW. Within this layer, PMW can form the largest component of near-glacier waters. Warm, salty AW entrained in the PMW warms near-glacier waters at intermediate depths, but acts counter to the initial input of freshwater. As such, subglacial-discharge plumes will increase submarine melting and the export of glacially modified waters to the shelf, but result in comparatively little change to the salinity stratification. The implications of this export for wider ocean circulation are thus likely very different to that of surface freshwater inputs, and should be assessed as a matter of priority.

Data Availability Statement

All data used in this study are freely available. NASA OMG CTD data are available from the PODAAC at https://podaac.jpl.nasa.gov/omg (OMG, 2020). BedMachine v5 is available from the NSIDC at https://nsidc.org/data/idbmg4/versions/5 (Morlighem et al., 2023). EN.4.2.2 data were obtained from https://www.metoffice.gov.uk/hadobs/en4/ (Good et al., 2023) and are © British Crown Copyright, Met Office, provided under a Non-Commercial Government Licence (http://www.nationalarchives.gov.uk/doc/non-commercial-government-licence/version/2/). Processed timeseries of meltwater runoff for each of the glacier catchments are available at https://doi.org/10.5281/zenodo.7696287 (Cowton, 2023a). The code for the plume and mixing models, along with scripts and data required to run these models for an example glacier, can be accessed at https://doi.org/10.5281/zenodo.8134725 (Cowton, 2023b).

References

Bartholomaus, T., Stearns, L., Sutherland, D., Shroyer, E., Nash, J., Walker, R., et al. (2016). Contrasts in the response of adjacent fjords and glaciers to ice-sheet surface melt in West Greenland. *Annals of Glaciology*, *57*(73), 1–14. https://doi.org/10.1017/aog.2016.19

Beaird, N., Straneo, F., & Jenkins, W. (2015). Spreading of Greenland meltwaters in the ocean revealed by noble gases. *Geophysical Research Letters*, *42*(18), 7705–7713. https://doi.org/10.1002/2015gl065003

Beaird, N. L., Straneo, F., & Jenkins, W. (2018). Export of strongly diluted Greenland meltwater from a major glacial fjord. *Geophysical Research Letters*, *45*(9), 4163–4170. https://doi.org/10.1029/2018gl077000

Bendtsen, J., Mortensen, J., Lennert, K., & Rysgaard, S. (2015). Heat sources for glacial ice melt in a west Greenland tidewater outlet glacier fjord: The role of subglacial freshwater discharge. *Geophysical Research Letters*, *42*(10), 4089–4095. https://doi.org/10.1002/2015gl063846

Bjørk, A. A., Kruse, L. M., & Michaelsen, P. B. (2015). Brief communication: Getting Greenland's glaciers right – A new data set of all official Greenlandic glacier names. *The Cryosphere*, *9*(6), 2215–2218. https://doi.org/10.5194/tc-9-2215-2015

Carroll, D., Sutherland, D. A., Hudson, B., Moon, T., Catania, G. A., Shroyer, E. L., et al. (2016). The impact of glacier geometry on meltwater plume structure and submarine melt in Greenland fjords. *Geophysical Research Letters*, *43*(18), 9739–9748. https://doi.org/10.1002/2016gl070170

Carroll, D., Sutherland, D. A., Shroyer, E. L., Nash, J. D., Catania, G. A., & Stearns, L. A. (2017). Subglacial discharge-driven renewal of tidewater glacier fjords. *Journal of Geophysical Research: Oceans*, *122*(8), 6611–6629. https://doi.org/10.1002/2017jc012962

Catania, G., Stearns, L., Moon, T., Enderlin, E., & Jackson, R. (2020). Future evolution of Greenland's marine-terminating outlet glaciers. *Journal of Geophysical Research: Earth Surface*, *125*(2), e2018JF004873. https://doi.org/10.1029/2018jf004873

Chauché, N., Hubbard, A., Gascard, J. C., Box, J. E., Bates, R., Koppes, M., et al. (2014). Ice-ocean interaction and calving front morphology at two west Greenland tidewater outlet glaciers. *The Cryosphere*, *8*(4), 1457–1468. https://doi.org/10.5194/tc-8-1457-2014

Cowton, T. (2023a). Modelled runoff for 14 glaciers in NW Greenland, 2015-2020 [Dataset]. Zenodo. https://doi.org/10.5281/zenodo.7696287

Cowton, T. (2023b). *tcowton/plume_modification: Plume_modification* (v1.0) [Software]. Zenodo. https://doi.org/10.5281/zenodo.8134725

Cowton, T., Sole, A., Nienow, P., Slater, D., Wilton, D., & Hanna, E. (2016). Controls on the transport of oceanic heat to Kangerdlugssuaq Glacier, east Greenland. *Journal of Glaciology*, *62*(236), 1167–1180. https://doi.org/10.1017/jog.2016.117

Davison, B. J., Cowton, T., Sole, A., Cottier, F., & Nienow, P. (2022). Modelling the effect of submarine iceberg melting on glacier-adjacent water properties. *The Cryosphere*, *16*(4), 1181–1196. https://doi.org/10.5194/tc-16-1181-2022

Fenty, I., Willis, J. K., Khazendar, A., Dinardo, S., Forsberg, R., Fukumori, I., et al. (2016). Oceans Melting Greenland: Early results from NASA's ocean-ice mission in Greenland. *Oceanography*, *29*(4), 72–83. https://doi.org/10.5670/oceanog.2016.100

Fried, M. J., Carroll, D., Catania, G. A., Sutherland, D. A., Stearns, L. A., Shroyer, E. L., & Nash, J. D. (2019). Distinct Frontal ablation processes drive heterogeneous submarine terminus morphology. *Geophysical Research Letters*, *46*(21), 12083–12091. https://doi.org/10.1029/2019GL083980

Golledge, N. R., Keller, E. D., Gomez, N., Naughten, K. A., Bernales, J., Trusel, L. D., & Edwards, T. L. (2019). Global environmental consequences of twenty-first-century ice-sheet melt. *Nature*, *566*(7742), 65–72. https://doi.org/10.1038/s41586-019-0889-9

Good, S. A., Martin, M. J., & Rayner, N. A. (2013). EN4: Quality controlled ocean temperature and salinity profiles and monthly objective analyses with uncertainty estimates. *Journal of Geophysical Research: Oceans*, *118*(12), 6704–6716. https://doi.org/10.1002/2013jc009067

Good, S. A., Martin, M. J., & Rayner, N. A. (2023). EN4.2.2 (.g10 bias corrections): Quality controlled ocean temperature and salinity profiles and monthly objective analyses with uncertainty estimates [Dataset]. Met Office. https://www.Metoffice.Gov.Uk/Hadobs/En4/

Gouretski, V., & Cheng, L. (2020). Correction for systematic errors in the global dataset of temperature profiles from mechanical bathythermographs. *Journal of Atmospheric and Oceanic Technology*, *37*(5), 841–855. https://doi.org/10.1175/jtech-d-19-0205.1

Gouretski, V., & Reseghetti, F. (2010). On depth and temperature biases in bathythermograph data: Development of a new correction scheme based on analysis of a global ocean database. *Deep Sea Research Part I: Oceanographic Research Papers*, *57*(6), 812–833. https://doi.org/10.1016/j.dsr.2010.03.011

Inall, M. E., Murray, T., Cottier, F. R., Scharrer, K., Boyd, T. J., Heywood, K. J., & Bevan, S. L. (2014). Oceanic heat delivery via Kangerdlugssuaq Fjord to the south-east Greenland ice sheet. *Journal of Geophysical Research-Oceans*, *119*(2), 631–645. https://doi.org/10.1002/2013jc009295

Jackson, R. H., Shroyer, E. L., Nash, J. D., Sutherland, D. A., Carroll, D., Fried, M. J., et al. (2017). Near-glacier surveying of a subglacial discharge plume: Implications for plume parameterizations. *Geophysical Research Letters*, *43*(13), 6886–6894. https://doi.org/10.1002/2017GL073602

Jackson, R. H., Straneo, F., & Sutherland, D. A. (2014). Externally forced fluctuations in ocean temperature at Greenland glaciers in non-summer months. *Nature Geoscience*, *7*(7), 503–508. https://doi.org/10.1038/ngeo2186

Jenkins, A. (2011). Convection-driven melting near the grounding lines of ice shelves and tidewater glaciers. *Journal of Physical Oceanography*, *41*(12), 2279–2294. https://doi.org/10.1175/jpo-d-11-03.1

Mankoff, K. D., Noël, B., Fettweis, X., Ahlstrøm, A. P., Colgan, W., Kondo, K., et al. (2020). Greenland liquid water discharge from 1958 through 2019. *Earth System Science Data*, *12*(4), 2811–2841. https://doi.org/10.5194/essd-12-2811-2020

Mankoff, K. D., Straneo, F., Cenedese, C., Das, S. B., Richards, C. G., & Singh, H. (2016). Structure and dynamics of a subglacial discharge plume in a Greenlandic Fjord. *Journal of Geophysical Research: Oceans*, *121*(12), 8670–8688. https://doi.org/10.1002/2016jc011764

McDougall, T. J., & Barker, P. M. (2011). Getting started with TEOS-10 and the Gibbs Seawater (GSW) oceanographic toolbox. *Scor/Iapso WG*, *127*, 1–28.

Morlighem, M., Williams, C. N., Rignot, E., An, L., Arndt, J. E., Bamber, J. L., et al. (2023). IceBridge BedMachine Greenland, version 5 [Dataset]. NASA National Snow and Ice Data Center Distributed Active Archive Center. https://doi.org/10.5067/GMEVBWFLWA7X

Morlighem, M., Williams, C. N., Rignot, E., An, L., Arndt, J. E., Bamber, J. L., et al. (2017). BedMachine v3: Complete bed topography and ocean bathymetry mapping of Greenland from multibeam echo sounding combined with mass conservation. *Geophysical Research Letters*, *44*(21), 11051–11061. https://doi.org/10.1002/2017gl074954

Morlighem, M., Wood, M., Seroussi, H., Choi, Y., & Rignot, E. (2019). Modeling the response of northwest Greenland to enhanced ocean thermal forcing and subglacial discharge. *The Cryosphere*, *13*(2), 723–734. https://doi.org/10.5194/tc-13-723-2019

Mortensen, J., Rysgaard, S., Bendtsen, J., Lennert, K., Kanzow, T., Lund, H., & Meire, L. (2020). Subglacial discharge and its down-fjord transformation in West Greenland fjords with an ice mélange. *Journal of Geophysical Research: Oceans*, *125*(9), e2020JC016301. https://doi.org/10.1029/2020jc016301

Muilwijk, M., Straneo, F., Slater, D. A., Smedsrud, L. H., Holte, J., Wood, M., et al. (2022). Export of ice sheet meltwater from Upernavik fjord, west Greenland. *Journal of Physical Oceanography*, *52*(3), 363–382. https://doi.org/10.1175/jpo-d-21-0084.1

Noël, B., van de Berg, W. J., Machguth, H., Lhermitte, S., Howat, I., Fettweis, X., & Van Den Broeke, M. R. (2016). A daily, 1 km resolution data set of downscaled Greenland ice sheet surface mass balance (1958–2015). *The Cryosphere*, *10*(5), 2361–2377. https://doi.org/10.5194/tc-10-2361-2016

O'Leary, M., & Christoffersen, P. (2013). Calving on tidewater glaciers amplified by submarine frontal melting. *The Cryosphere*, *7*(1), 119–128. https://doi.org/10.5194/tc-7-119-2013

OMG. (2020). OMG CTD conductivity temperature depth [Dataset]. Ver. 1. PO.DAAC. https://doi.org/10.5067/OMGEV-CTDS1

Shreve, R. L. (1972). Movement of water in glaciers. *Journal of Glaciology*, *11*(62), 205–214. https://doi.org/10.3189/s002214300002219x

Slater, D., Benn, D., Cowton, T., Bassis, J., & Todd, J. (2021). Calving multiplier effect controlled by melt undercut geometry. *Journal of Geophysical Research: Earth Surface*, *126*(7), e2021JF006191. https://doi.org/10.1029/2021jf006191

Slater, D., Carroll, D., Oliver, H., Hopwood, M., Straneo, F., Wood, M., et al. (2022). Characteristic depths, fluxes and timescales for Greenland's tidewater glacier fjords from subglacial discharge-driven upwelling during summer. *Geophysical Research Letters*, *49*(10), e2021GL097081. https://doi.org/10.1029/2021gl097081

Slater, D. A., Felikson, D., Straneo, F., Goelzer, H., Little, C. M., Morlighem, M., et al. (2020). Twenty-first century ocean forcing of the Greenland ice sheet for modelling of sea level contribution. *The Cryosphere*, *14*(3), 985–1008. https://doi.org/10.5194/tc-14-985-2020

Slater, D. A., Goldberg, D. N., Nienow, P. W., & Cowton, T. R. (2016). Scalings for submarine melting at tidewater glaciers from buoyant plume theory. *Journal of Physical Oceanography*, *46*(6), 1839–1855. https://doi.org/10.1175/jpo-d-15-0132.1

Stevens, L. A., Straneo, F., Das, S. B., Plueddemann, A. J., Kukulya, A. L., & Morlighem, M. (2016). Linking glacially modified waters to catchment-scale subglacial discharge using autonomous underwater vehicle observations. *The Cryosphere*, *10*(1), 417–432. https://doi.org/10.5194/tc-10-417-2016

Straneo, F., Curry, R. G., Sutherland, D. A., Hamilton, G. S., Cenedese, C., Vage, K., & Stearns, L. A. (2011). Impact of fjord dynamics and glacial runoff on the circulation near Helheim Glacier. *Nature Geoscience*, *4*(5), 322–327. https://doi.org/10.1038/ngeo1109

Straneo, F., Sutherland, D. A., Holland, D., Gladish, C., Hamilton, G. S., Johnson, H. L., et al. (2012). Characteristics of ocean waters reaching Greenland's glaciers. *Annals of Glaciology*, *53*(60), 202–210. https://doi.org/10.3189/2012AoG60A059

Sutherland, D., Straneo, F., Moon, T., Le Bras, I., Frajka-Williams, E., Bamber, J., et al. (2018). Freshwater fluxes from the Greenland ice sheet: Report from an international workshop.

Swingedouw, D., Houssais, M.-N., Herbaut, C., Blaizot, A.-C., Devilliers, M., & Deshayes, J. (2022). AMOC recent and future trends: A crucial role for oceanic resolution and Greenland melting? *Frontiers in Climate*, *4*. https://doi.org/10.3389/fclim.2022.838310

Zhao, K. X., Stewart, A. L., & McWilliams, J. C. (2021). Geometric constraints on glacial fjord–shelf exchange. *Journal of Physical Oceanography*, *51*(4), 1223–1246. https://doi.org/10.1175/jpo-d-20-0091.1